Type of contribution:
Editorial
▶ Research Paper
Case Study
Review Paper
Scientific Data
Report of Tech. Application

e-issn. 2798-5245
Mechanical Engineering for Society and Industry
Vol. 5, No. 1 (2025) pp 276-285
https://doi.org/10.31603/mesi.13314

Ballistic performance of a composite armor reinforced by alumina balls with various matrix materials: A numerical study

Agustinus Andrie Prasetyo[1], Aditya Praba Wijaya[1], Desi Gustiani[2], Akida Mulyaningtyas[1], Tri Widodo Besar Riyadi[1]*

[1] Faculty of Engineering, Universitas Muhammadiyah Surakarta, Sukoharjo 57102, **Indonesia**
[2] Department of Mechanical Engineering, Faculty of Technology, Sakarya University of Applied Sciences, **Türkiye**
✉ tri.riyadi@ums.ac.id

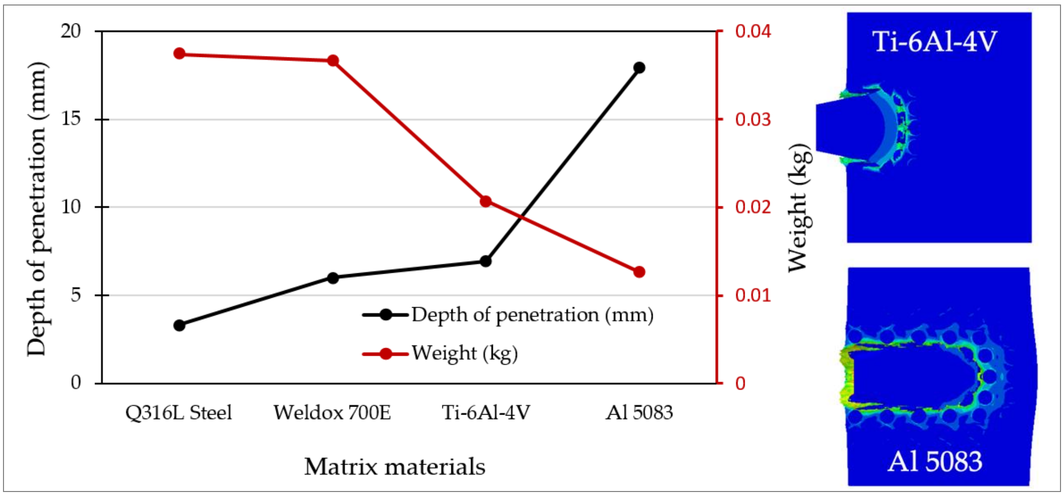

Highlights:
- A ballistic test of alumina ball composites was simulated using Abaqus software.
- The composite's matrix comprises Al 5083, Ti-6Al-4V, Weldox 700E, and Q235 steel.
- Increasing the Young's modulus decreases the depth of penetration.
- Higher and lower Young's modulus form mushrooming and ductile hole, respectively.

Article info
Submitted: 2025-03-14
Revised: 2025-06-27
Accepted: 2025-06-28

Publisher
Universitas Muhammadiyah Magelang

Abstract
This study observed the ballistic performance of the composite armor reinforced by an alumina ball with various matrix materials. The investigation was conducted numerically to establish an effective design of the composite armor for protection against a 7.62 mm bullet impacting at 800 m/s speed. Al 5083, Ti-6Al-4V, Weldox 700E, and Q235 steel, along with ceramic balls acting as reinforcement, make up the composite. The simulation was set in a 3D model and performed using Abaqus finite element software. The outputs of the simulation present the residual velocity, the depth of penetration, the optimized weight-to-penetration depth ratio, and the deformation pattern. The results indicated that the composite armor with ceramic ball reinforcement produced the optimum design using a matrix of Ti-6Al-4V. The matrix with a higher Young modulus has a higher velocity decrease. The matrix with a higher plastic equivalent strength has a higher resistance to the projectile deformation, marked by mushrooming during its penetration. On the contrary, the matrix with a lower plastic equivalent strength forms a ductile hole. This work guides to determination of the optimal design of composite armor containing ceramic balls as reinforcement, considering the different matrix materials.

Keywords: Ballistic simulations; Ceramic balls; Matrix materials; Depth of penetration; Panel's weight

1. Introduction

Ballistic armor has been used as a protective device for the human body or military vehicle against a bullet strike. To improve the ballistic performance, the armor material needs to have high strength, lightweight, and high hardness [1]. The structure of conventional armor generally uses ceramic materials such as SiC, B_4C, and Al_2O_3 as the front panel, whereas metal or resin is widely used as the back panel. However, the front structure with a single ceramic layer is very susceptible to overall damage because ceramics are brittle, especially when the panel experiences repeated bullet shots. Composite materials provide superior performance by integrating the features of their constituent components [2]. Composite materials can improve the armor's strength since ceramic particles are wrapped by a matrix of metal or resin materials, which have better ballistic resistance compared to layered structures because they can absorb the higher kinetic energy of the bullets [3].

Composite structures are not able to withstand the impact load from bullet shots that have an angle of inclination to the normal plane of the panel. If the bullet is fired at an angle from the panel plane, the panel's resistance decreases. Recently, researchers found a composite bulletproof panel with ceramic ball reinforcement to increase the panel's resistance to angular impact loads [4]. The reinforcement material from these ceramic balls is wrapped in a soft metal matrix or resin as a binder to form a composite structure. The metal matrix provides ductility and strengthening, preventing the ceramic balls from fracturing and enabling the panel to withstand several hits. The metal matrix also serves as a support structure for the ceramic balls, dispersing forces and preventing their collapse [5]. On the contrary, the advantage of the ceramic ball panel structure is the curved texture of the ball surface, which can provide asymmetric resistance to the bullet impact load so that it can change the direction of its ballistic trajectory. Consequently, the bullet's kinetic energy will decrease, leading to a reduction in the depth of bullet penetration [6].

Technological inventions relating to bulletproof panels made of composite materials with ceramic ball reinforcement have been reported in some studies using both experimental and numerical methods. Amongst the kinds of ceramic balls, alumina has some high advantages for ballistic purposes [7]. Alumina ceramic balls possess high compressive strength and hardness, allowing them to erode and break the projective tip during impact. The fragmented projectile decreases the penetrating depth [8]. In addition, alumina ceramics are comparatively more lightweight than other materials, resulting in comfort for mobility [4].

Kang *et al*. [5] studied the penetration process of a composite armor with ceramic balls/UHPC panel under a 10 mm armor-piercing projectile. The effect of ball diameter and the ball number on the panel resistance under impact was observed. The results show that the UHPC matrix delivers good constraint on the ceramic balls, which increases their impact resistance. The simulation using ANSYS/LS-DYNA enables discussion of the changes in damage and kinetic energy during impact. The model allows the selection of the optimum diameter of a ceramic ball with various projectile diameters.

Ansari *et al*. [9] reported the ballistic performance of a composite armor with Al5083 aluminum alloy as the matrix and alumina balls as the reinforcement. The Abaqus FE code was used to simulate the depth of penetration, residual velocity, and kinetic energy of the plates under the impact of a 7.62 mm projectile at 800 m/s speed. The effect of ceramic balls with 15%, 30%, and 45% weight percentages and the plate's thickness of 20, 25, and 30 mm was investigated. The results show that the highest ballistic performance was achieved when using the composite plate with a ball weight percentage of 30% and a thickness of 25 mm.

Akbari *et al*. [10] investigated the ballistic behavior of composite plates comprising AA6061, AA7075, and Al5083 aluminum alloys matrix reinforced by alumina ball with 15%, 30%, and 45% weight percentages. Simulation models of the panels against 7.62 × 39 mm projectiles were executed using Abaqus FE code and validated using experimental tests. The residual velocity, penetration depth, kinetic energy, and projectile erosion were observed on the panel with thicknesses of 20, 25, and 30 mm. The results demonstrate that the AA5083 materials give the highest ballistic performance, while AA6061 is the lowest one.

Considering that the matrix material plays an important role in the ballistic performance of the composite plates reinforced by ceramic balls, as observed by Akbari *et al*. [10], it is then necessary to expand to more different materials that can improve the ballistic performance of the armor. Although many works have studied the variation of different matrix materials in the composite reinforced by alumina balls, most of them only use aluminum as the matrix. There are still a few that explore various metal materials such as steel and titanium alloys. In response to this limited study, this work conducted a simulation on the ballistic performance of a composite plate with various matrix materials and alumina ceramic balls as the reinforcement. An Abaqus FE code was used to simulate the ballistic impact of a 7.62 mm projectile on the composite plate with various matrix materials. The simulation results were validated based on research conducted by Ansari *et al*. [9]. The model can be used to determine the ballistic performance of the armor design, which also provides references for further research.

2. Simulation Methods

2.1. Simulation Procedure

In this simulation work, Abaqus/Explicit Dynamic [11] was used to observe the ballistic behavior of a composite panel with the reinforcements of alumina balls and the matrix consisting of Al 5083, Ti-6Al-4V, Weldox 700E, and Q235 steel against the impact of a 7.62 mm projectile load at 800 m/s speed. The models were employed to describe the projectile (**Figure 1**) and the panel (**Figure 2**), which is in accordance with that used in the study conducted by Ansari *et al*. [9]. The projectile has a length of 28 mm and a radius of 4 mm, achieving a mass of 8 gr. On the other side, the panel has an area of 15 mm x 15 mm and a thickness of 25 mm. The models were made in 3D axisymmetric by taking 1/4 parts of the real model to reduce computational costs. Alumina balls with a diameter of 2 mm are arranged evenly in the matrix, with an arrangement as shown in **Figure 3**. The mechanical contact between the matrix and the alumina balls is regarded as tie. The tied contact model can demonstrate the value of maximum stress that aligns with experimental findings [12]. In general, the present models are similar to those reported by Ansari *et al*. [9] for comparison purposes.

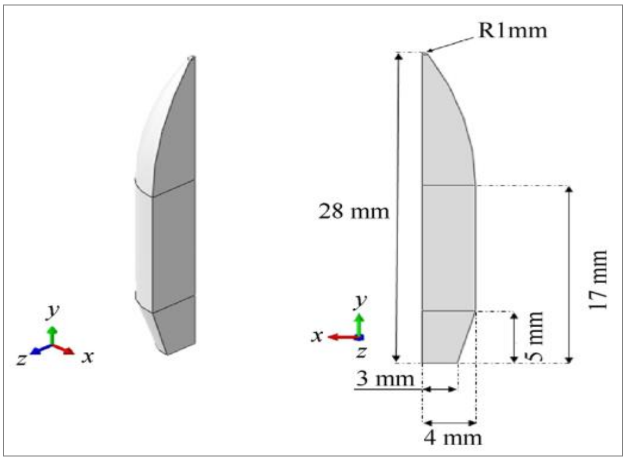

Figure 1.
Projectile dimension

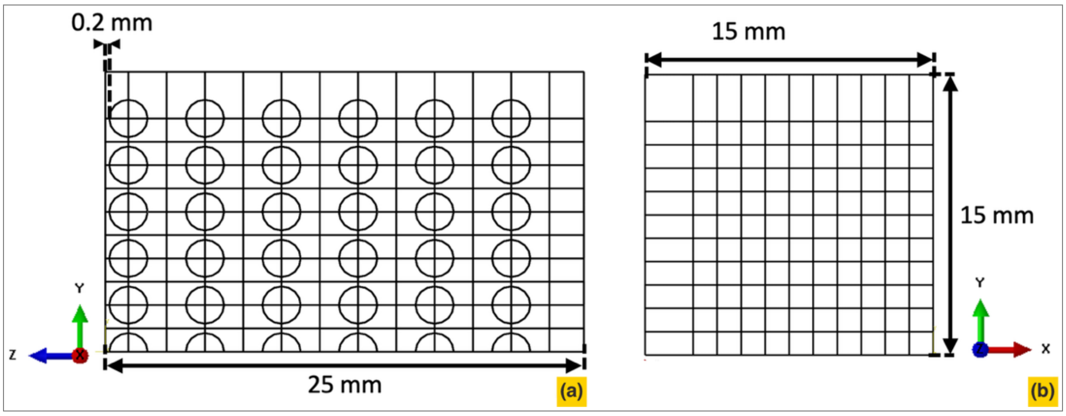

Figure 2.
Armor dimension:
(a) Side view;
(b) Front view

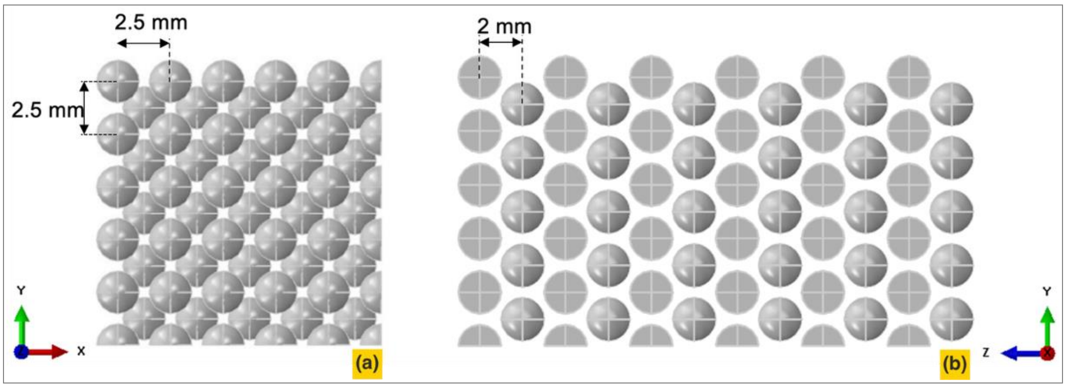

Figure 3.
Configuration of alumina balls in the matrix:
(a) Side view;
(b) Front view

Figure 4 shows the boundary conditions of the model, which is adjusted to adopt the constraints to the sample that occurred in the experimental conditions. In **Figure 4a**, the outer side of the armor is fixed to ensure that all faces on that side do not move at all, marked with U1=U2=U3=UR1=UR2=UR3=0, which means that the element moves both translation and rotation by 0 mm on the x, y, and z-axes. **Figure 4b** shows the axisymmetric section, symbolized by U1=UR2=UR3=0, which means that the sides of the element do not move in the x-axis direction. U2=UR1=UR3=0 means that the sides of the element do not move in the y-axis direction. The projectile load is given a speed of 800 m/s, moving in the z-axis.

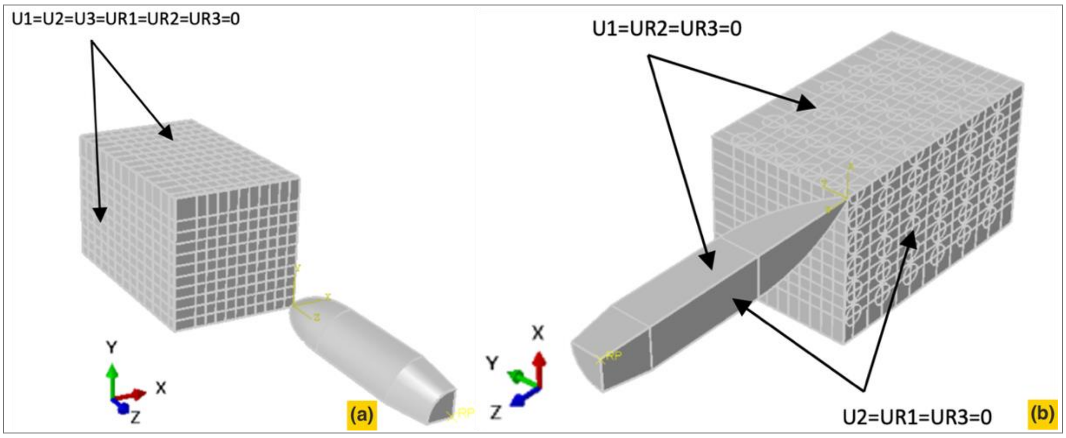

Figure 4. Boundary conditions of the panel and projectile: (a) Outer sides; (b) Internal sides

For modeling the deformation of the metal materials, Johnson-Cook parameters were used, as given in **Table 1**. On the other side, Johnson-Holmquist properties are used for modeling the material failure of ceramic materials, as given in **Table 2**. Since Abaqus does not have a Johnson-Holmquist material library, similar properties are used, namely the Drucker-Prager plastic model and Mie-Gruneisen equation of state (EOS), as given in **Table 3** and **Table 4** [9], [13].

Table 1. Material properties of Al 5083, Ti-6Al-4V, Weldox 700E, Q235 steel, and Steel 4340

Parameter, symbol	Unit	Values				
		Al 5083 [14]	Ti-6Al-4V [15]	Weldox 700E [16]	Q235 Steel [17]	Steel 4340 [14]
Mechanical properties						
Density, ρ	kg/m³	2976	4883	8653	7830	8598
Poisson's Ratio, ν	-	0.3	0.33	0.33	0.29	0.3
Young Modulus, *E*	MPa	70000	110000	210000	210000	21000
Shear Modulus, *G*	MPa	26900	-	-	-	81800
Johnson Cook Strength						
Initial Yield Stress, *A*	MPa	167	862	859	235	792
Hardening Constant, *B*	MPa	596	331	329	400	510
Hardening Exponent, *n*	-	0.551	0.34	0.579	0.36	0.26
Strain Rate Constant, *C*	-	0.001	0.012	0.0115	0.039	0.014
Thermal Softening, *m*	-	0.859	0.8	1.071	0.55	1.03
Melting Temperature, T_m	°C	893	1630	1800	1795	1793
Johnson Cook Failure						
Damage Constant D1	-	0.0261	-0.09	0.361	0.3	0.05
Damage Constant D2	-	0.263	0.25	4.768	0.9	3.44
Damage Constant D3	-	-0.349	-0.5	-5.107	-2.8	-2.12
Damage Constant D4	-	-0.247	0.014	-0.0013	0	0.002
Damage Constant D5	-	16.8	3.87	1.333	0	0.61
Melting Temperature	°C	893	1630	1800	1795	1793

Table 2. Material properties of Alumina [9]

Parameters	Symbol	Value	Unit
Density	ρ	3890	kg/m³
Shear modulus	*G*	152	GPa
Constant	α	0.0017356	-
Constant	b	1.5625	-
Compressive strength	σ_c	12227.4626	MPa
Strain rate coefficient	C	0.007	-
Specific heat coefficient	C_p	880	J/Kg.K

Table 3. Alumina drucker-prager plasticity model [9]

Stress triaxiality	Plastic strain at failure
-1.2741185	2.0375607
-0.8906344	0.54057149
-0.84331	0.44183511
-0.7401157	0.27310304
-0.6208802	0.14341538
-0.4739009	5.39e-2
-0.2545951	6.59e-3
-0.2383005	5.38e-3
-0.2016224	3.33e-3
-0.1561862	1.75e-3
-9.11e-2	6.57e-4
6.93e-2	8.02e-5
8.92e-2	6.56e-5
0.22966913	2.13e-5
1.22975016	9.77e-7

Table 4. Mie-Gruneisen EOS parameters of Al 5083, steel 4340, dan Alumina [9]

Parameter	Notation	Al5083	Steel 4340	Alumina
Slop in U_s versus U_p diagram	S	1.338	1.49	0.15368
Gruneisen coefficient	γ_0	2	2.17	1.7
Elastic wave speed (m/s)	C_0	5330	4569	7706.038

2.2. Mesh Convergence

In a simulation using finite element software, the smaller the mesh size, the more accurate the simulation results obtained. However, the smaller the mesh size, the longer the computation time required [18]. Mesh convergence studies need to be conducted to determine the mesh size that has a balance between accuracy and computation time [19]. The mesh sizes used in this study were 1, 0.5, 0.45, 0.35, 0.3, 0.27, and 0.25 with output in the form of residual velocity. **Figure 5**, showing the simulation results, indicates that at a mesh size of 0.3, the residual velocity value begins to be consistent, followed by mesh sizes of 0.27 and 0.25. However, the smaller the mesh size, the number of elements increases. Therefore, a mesh size of 0.3 was chosen in this study.

Modeling metal materials requires Johnson-Cook parameters to predict the material deformation. Similarly, ceramic materials use Johnson-Holmquist properties to predict material failure. Since Abaqus does not have a Johnson-Holmquist material library, this study uses similar properties, specifically the Drucker-Prager plastic model and the Mie-Gruneisen Equation of State (EOS) [9]. This property plays a role in predicting material damage in shock wave, ballistic, and blast studies. However, the Mie-Gruneisen Equation of state (EOS) material property is not found in various literature. An alternative solution is to use the Johnson-Cook Constitutive Model. Therefore, it is necessary to validate the use of the two material models. **Figure 6** shows a comparison of the simulation results on residual velocity using the Mie-Gruneisen EOS model and Johnson Cook, which is applied to three plates (**Figure 7**). The simulation results show that there is no significant difference in residual velocity with the use of the Mie-Gruneisen EOS material model with Johnson Cook.

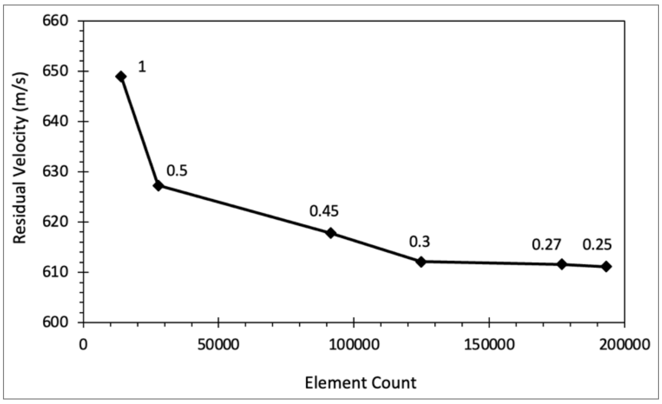

Figure 5. Mesh convergence

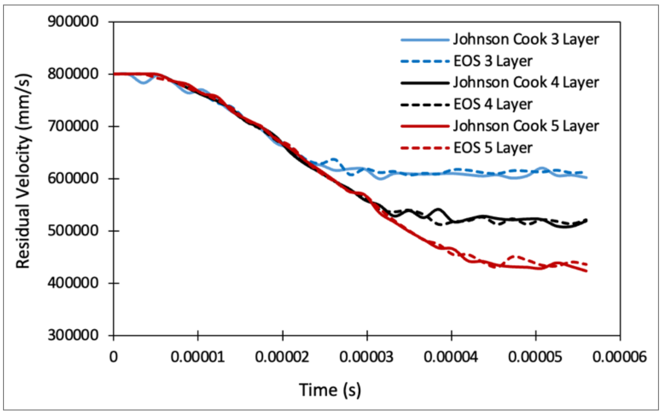

Figure 6. Model comparison between Johnson Cook and Mie-Gruneisen Equation of state (EOS)

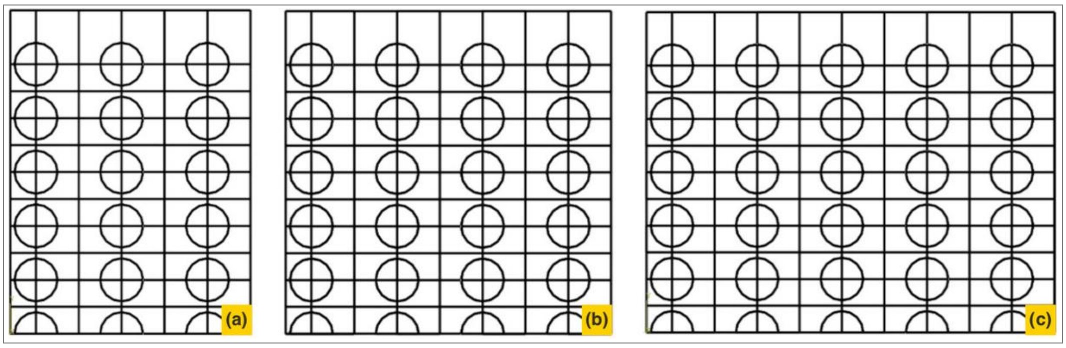

Figure 7. Panel thickness with ceramic balls comprising: (a) 3 layers; (b), 4 layers; (c) 5 layers

2.3. Validation

To find out that the model used in the simulation has sufficient accuracy, verification is carried out by comparing the simulation results with the experiment results of other studies. In this simulation, the depth of penetration (DOP) from the simulation results are compared with the results of experiments conducted by Ansari *et al*. [9], who conducted three ballistic tests on panels with Al 5083 matrix material and ceramic ball reinforcement of 30% by weight. The experimental results produced a DOP of 18.65 mm, 19.20 mm, and 18.35 mm so the average DOP is 18.73 mm.

In addition to the experiment, Ansari also conducted a simulation using Abaqus software, which produced a DOP of 20.57 mm. While the current simulation produces a DOP of 17.87 mm. **Table 5** shows the results of the DOP comparison between the simulation conducted by Ansari and the current simulation against the results of Ansari's experiment. The comparison indicates that the current simulation result deviates by 4.19% from Ansori's experimental result. On the contrary, Ansori's simulation exhibits a 9.80% deviation from their experimental results. To sum up, the present simulation results exhibit a lesser discrepancy from Ansori's experiment than from Ansori's simulation. Therefore, the selected modeling in this work can be used for further observation, particularly, to evaluate the effect of the matrix materials.

Table 5. Verification of the depth of penetration

	Experiment by [9]	Simulation by [9]	Present simulation
Depth of penetration (mm)	18.73	20.57	17.87
Difference to experiment (%)	-	9.80	4.19

3. Results and Discussion

3.1. Profile of the Projectile Velocity

Figure 8 shows the velocity profile of the projectile when it first hits the panel, specifically at time t = 0. All the projectile velocity curves decrease with increasing time. This decrease indicates the absorption of the projectile's kinetic energy by the armor plate, which causes its speed to decrease. When the curve reaches a projectile velocity of 0 m/s, the projectile stops motion. The results indicate that at t = 70 µs, all projectile velocities have diminished to zero, signifying that no projectiles penetrate the panel beyond that moment. Certain projectile velocity curves exhibit negative values, signifying a rebound in the opposite direction or reflection from a particular distance. This scenario may occur if the projectile's kinetic energy is inadequate to penetrate the armor or if the projectile is distorted.

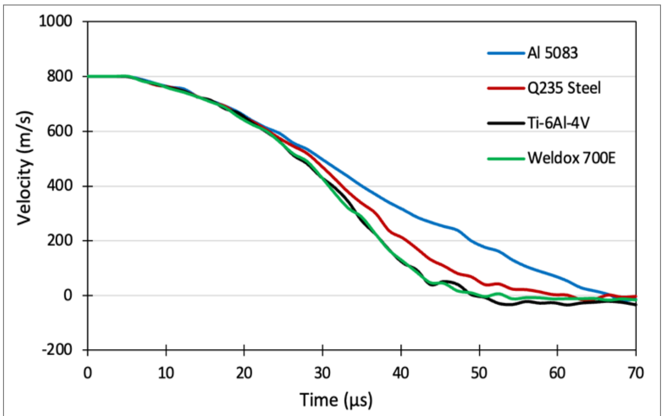

Figure 8. Profile of projectile velocity in the panel with different matrix materials

Comparing the projectile velocity in the panel with different matrix materials, the velocity decrease in the panel with a matrix material of Ti-6Al-4V and Weldox 700E is faster than that of Al 5083. This comparison indicates that the Ti-6Al-4V and Weldox 700E matrix absorb more kinetic energy than Al 5083. The absorption of kinetic energy by the panel can be associated with the Young's modulus value of the material. In matrix materials that have high Young's modulus values, they tend to have higher stiffness properties so that they are not easily deformed [20], [21]. As a result, the absorption of kinetic energy is greater so that it can be faster in reducing the speed of the projectile. Referring to **Table 1**, the Young modulus values of Ti-6Al-4V and Weldox 700E are 110000 MPa and 210000 MPa, respectively, while the Young modulus of Al 5083 is smaller, specifically 70000 MPa.

3.2. Depth of Penetration (DOP) Profile

Figure 9 shows the DOP curve profile of the panel with various matrix materials, where DOP increases with increasing time. A comparison between DOP curve profiles shows that the highest DOP increase is experienced by the Al 5083 matrix, while the lowest DOP increase is experienced by the Ti-6Al-4V and Weldox 700E matrices. This condition can be associated with the Young's modulus value, as also experienced by the velocity profile in **Figure 8**. Increasing the Young's modulus value will decrease the DOP. Yu *et al*. [7] reported that the ballistic performance of panels improves with increased Young's modulus. A material with a higher modulus has higher stiffness that absorbs higher impact energy, consequently lowering the penetration depth.

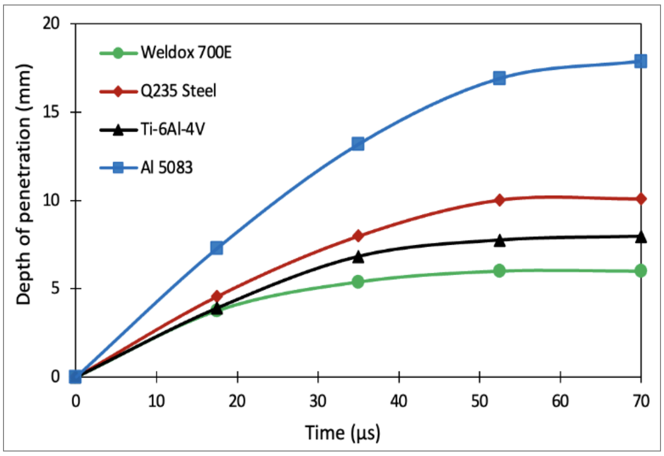

Figure 9. Profile of the projectile's penetration depth

3.3. DOP and Panel's Weight Ratio

Depth of penetration (DOP) is one of the important parameters for evaluating the performance of bulletproof plates, besides the weight of the panel [3]. **Figure 10** shows the DOP curve and panel's weight with variations in matrix material. Comparing the four matrix materials, the Q316L steel matrix has the lowest DOP but has the highest weight. Meanwhile, the Al 5083 matrix has the smallest weight but has the highest DOP. By considering the DOP and panel weight factors, the Ti-6Al-4V matrix has the best values, which have small DOP and weight. This finding agrees with that observed by Lui *et al*. [22], who demonstrate that Ti-6Al-4V is perfect for lightweight armor due to its high strength-to-weight ratio. This property makes robust, light armor possible and improves mobility due to its lower load.

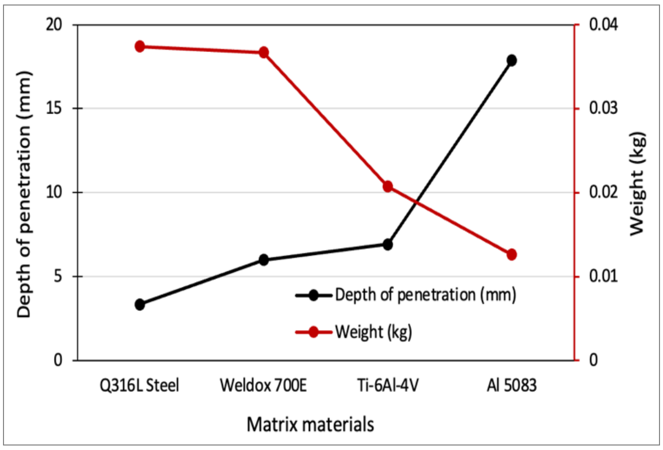

Figure 10. Optimization of the depth of penetration to the panel's weight

3.4. Panel's Deformation

Figure 11 illustrates the deformation pattern observed on the panel composed of Ti-6Al-4V and Al 5083 matrix materials at penetration times of 0 μs, 17.5 μs, 35 μs, 52.5 μs, and 70 μs. This study presents the deformation pattern as indicated by the plastic equivalent strength (PEEQ) value, reflecting the material's capacity for plastic deformation. PEEQ relates to energy absorption during the impact process. Materials exhibiting high PEEQ demonstrate enhanced energy absorption capabilities, thereby mitigating the potential of catastrophic failure [23]. A higher Young's modulus signifies increased resistance to penetration, requiring greater energy for the same penetration depth. Thus, a material with a higher Young's modulus will absorb more energy during indentation than the lower one [24].

In **Figure 11**, Ti-6Al-4V and Al 5083 matrix materials are chosen to show quite different deformation patterns. In the Al 5083 matrix, penetration causes deformation that is almost the same as the diameter of the projectile cross-section. This shows that the deformation in the Al 5083 material is caused by the low Young's modulus. This phenomenon can be called a ductile hole, which is in line with the study conducted by Rosenberg *et al*. [19].

In the Ti-6Al-4V matrix, the projectile penetrates, and erosion occurs starting at 17.5 μs. At this stage, both the matrix and the alumina ball play an important role in blunting the sharp tip of the projectile and reducing its penetration ability. At 35 μs to 52.5 μs, the penetration process is still ongoing at a decreasing speed, and plastic deformation begins to occur at the tip of the projectile. The mushrooming phenomenon occurs by widening the tip of the projectile and shortening the length of the projectile in the longitudinal direction [25]. The mushrooming that appeared in the Ti-6Al-4V matrix is not seen in the Al 5083 matrix. Increasing hardness might decrease the mushrooming ductility [26].

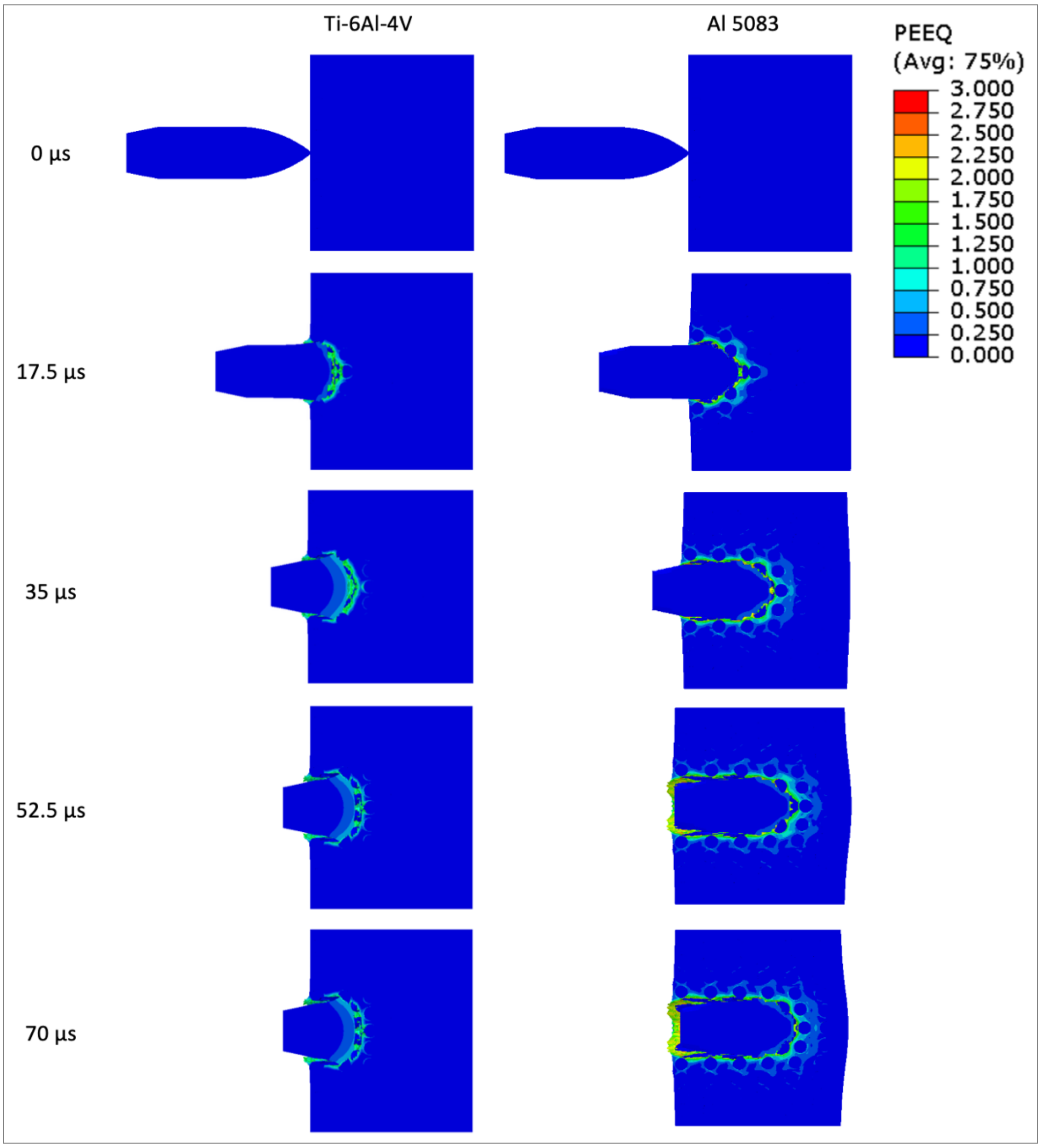

Figure 11. Deformation pattern in the panel using Ti-6Al-4V and Al 5083 matrices with higher and lower Young's modulus, respectively

4. Conclusion

This work has successfully investigated the ballistic performance of composite armors with ceramic ball reinforcement. The composite's matrix materials consist of Al 5083, Ti-6Al-4V, Weldox 700E, and Q235 steel. The experiment was conducted numerically using Abaqus/Explicit dynamic software to simulate the impact of a 7.62 mm projectile on the composite panel at a speed of 800 m/s. The simulation results were validated using those as observed by the experiment reported by Ansari et al. The projectile velocity indicates that the velocity decrease in the panel with a matrix material of Ti-6Al-4V and Weldox 700E is faster than that of Al 5083, which can be associated with the increased energy absorption with higher Young's modulus. A material with a greater Young's modulus exhibits increased stiffness, which absorbs more impact energy, consequently reducing penetration depth. The panel with Ti-6Al-4V and Weldox 700E matrices experiences the lowest penetration depth, which is related to the lower Young's modulus. Among the observed matrix materials, Ti-6Al-4V is the best optimum matrix concerning the penetration depth and panel weight. Young's modulus also plays an important role in the deformation pattern. A material with a low Young's modulus is subjected to a ductile hole during projectile impact. On the contrary, the panel with higher Young's modulus tends to form mushrooming occurrences. The present finding reports an improved ballistic performance of composite armors with ceramic ball reinforcement by replacing the Al 5083 matrix used in previous work with the Ti-6Al-4V matrix.

Authors' Declaration

Authors' contributions and responsibilities - The authors made substantial contributions to the conception and design of the study. The authors took responsibility for data analysis, interpretation and discussion of results. The authors read and approved the final manuscript.

Funding – The authors express gratitude to the Directorate General of Higher Education, Research, and Technology, Ministry of Education, Culture, and Technology, Republic of Indonesia, for grant No. 182/E5/PG.02.00.PL/2023 and 006/LL6/PB/AL.04/2023, 170.48/C.1-III/LRI/VI/2023.

Availability of data and materials – All data is available from the authors.

Competing interests – The authors declare no competing interests.

Additional information – No additional information from the authors.

References

[1] M. Y. Yaakob, M. P. Saion, and M. A. Husin, "Potency of natural and synthetic composites for ballistic resistance: A review," *Applied Research and Smart Technology (ARSTech)*, vol. 1, no. 2, pp. 43–55, Nov. 2020, doi: 10.23917/arstech.v1i2.52.

[2] R. Widyorini, N. H. Sari, M. Setiyo, and G. Refiadi, "The Role of Composites for Sustainable Society and Industry," *Mechanical Engineering for Society and Industry*, vol. 1, no. 2, pp. 48–53, 2021, doi: 10.31603/mesi.6188.

[3] Y. X. Zhai, H. Wu, and Q. Fang, "Impact resistance of armor steel/ceramic/UHPC layered composite targets against 30CrMnSiNi2A steel projectiles," *International Journal of Impact Engineering*, vol. 154, no. September 2020, 2021, doi: 10.1016/j.ijimpeng.2021.103888.

[4] W. zhan Wang, Z. gang Chen, S. shan Feng, and T. yong Zhao, "Experimental study on ceramic balls impact composite armor," *Defence Technology*, vol. 16, no. 2, pp. 408–416, 2020, doi: 10.1016/j.dt.2019.09.004.

[5] N. Kang, J. Lai, J. Zhou, L. Du, and J. Cao, "Effect of ceramic balls/UHPC panel on impact resistance of composite armor," *International Journal of Impact Engineering*, vol. 178, no. April, p. 104623, 2023, doi: 10.1016/j.ijimpeng.2023.104623.

[6] J. Liu, C. Wu, J. Li, J. Fang, Y. Su, and R. Shao, "Ceramic balls protected ultra-high performance concrete structure against projectile impact–A numerical study," *International Journal of Impact Engineering*, vol. 125, no. June 2018, pp. 143–162, 2019, doi: 10.1016/j.ijimpeng.2018.11.006.

[7] A. Z. Ziva, Y. K. Suryana, Y. S. Kurniadianti, R. Ragadhita, A. B. D. Nandiyanto, and T. Kurniawan, "Recent Progress on the Production of Aluminum Oxide (Al2O3) Nanoparticles: A Review," *Mechanical Engineering for Society and Industry*, vol. 1, no. 2, pp. 54–77, 2021, doi: 10.31603/mesi.5493.

[8] H. Dahlan, "the Effect of Critical Traction in Cohesive Zone Model for Fatigue Crack Growth Retardatio," *Media Mesin: Majalah Teknik Mesin*, vol. 17, no. 2, pp. 44–54, 2016, doi: 10.23917/mesin.v17i2.2883.

[9] A. Ansari, T. Akbari, and M. R. Pishbijari, "Investigation on the ballistic performance of the aluminum matrix composite armor with ceramic balls reinforcement under high velocity impact," *Defence Technology*, no. xxxx, pp. 1–19, 2023, doi: 10.1016/j.dt.2023.01.015.

[10] T. Akbari, A. Ansari, and M. Rahimi Pishbijari, "Influence of aluminum alloys on protection performance of metal matrix composite armor reinforced with ceramic particles under

ballistic impact," *Ceramics International*, vol. 49, no. 19, pp. 30937–30950, 2023, doi: 10.1016/j.ceramint.2023.07.046.

[11] T. W. B. Riyadi and W. A. Siswanto, "The use of Abaqus for teaching the development of cavity defects in forward extrusion processes," *International Journal of Mechanical Engineering Education*, vol. 36, no. 3, pp. 221–224, 2008, doi: 10.7227/IJMEE.36.3.5.

[12] Mujiyono, H. K. Perdana, D. Nurhadiyanto, V. H. L. Saputri, and S. A. Hassan, "Analysis of Load and Contact Mechanic on the Composite Structural: Case Study on Gfrp Composite," *EUREKA, Physics and Engineering*, vol. 2024, no. 4, pp. 133–143, 2024, doi: 10.21303/2461-4262.2024.003269.

[13] J. Chen, W. Chen, S. Chen, G. Zhou, and T. Zhang, "Shock Hugoniot and Mie-Grüneisen EOS of TiAl alloy: A molecular dynamics approach," *Computational Materials Science*, vol. 174, no. January, p. 109495, 2020, doi: 10.1016/j.commatsci.2019.109495.

[14] A. Rashed, M. Yazdani, A. A. Babaluo, and P. Hajizadeh Parvin, "Investigation on high-velocity impact performance of multi-layered alumina ceramic armors with polymeric interlayers," *Journal of Composite Materials*, vol. 50, no. 25, pp. 3561–3576, 2016, doi: 10.1177/0021998315622982.

[15] Y. Zhang, J. C. Outeiro, and T. Mabrouki, "On the selection of Johnson-Cook constitutive model parameters for Ti-6Al-4V using three types of numerical models of orthogonal cutting," *Procedia CIRP*, vol. 31, pp. 112–117, 2015, doi: 10.1016/j.procir.2015.03.052.

[16] S. Dey, T. Børvik, O. S. Hopperstad, J. R. Leinum, and M. Langseth, "The effect of target strength on the perforation of steel plates using three different projectile nose shapes," *International Journal of Impact Engineering*, vol. 30, no. 8–9, pp. 1005–1038, 2004, doi: 10.1016/j.ijimpeng.2004.06.004.

[17] F. lin Zhu, Y. Chen, and G. li Zhu, "Numerical simulation study on penetration performance of depleted Uranium (DU) alloy fragments," *Defence Technology*, vol. 17, no. 1, pp. 50–55, 2021, doi: 10.1016/j.dt.2020.01.002.

[18] M. N. Ibrahim, W. A. Siswanto, and A. M. A. Zaidi, "Computational issues in the simulation of high speed ballistic impact: A Review," *Applied Mechanics and Materials*, vol. 315, no. April 2013, pp. 762–767, 2013, doi: 10.4028/www.scientific.net/AMM.315.762.

[19] A. Ghavidel, M. Rashki, H. Ghohani Arab, and M. Azhdary Moghaddam, "Reliability mesh convergence analysis by introducing expanded control variates," *Frontiers of Structural and Civil Engineering*, vol. 14, no. 4, pp. 1012–1023, 2020, doi: 10.1007/s11709-020-0631-6.

[20] J. He, L. He, and B. Yang, "Analysis on the impact response of fiber-reinforced composite laminates: An emphasis on the FEM simulation," *Science and Engineering of Composite Materials*, vol. 26, no. 1, pp. 1–11, 2019, doi: 10.1515/secm-2017-0222.

[21] T. L. Chu, C. Ha-Minh, and A. Imad, "A numerical investigation of the influence of yarn mechanical and physical properties on the ballistic impact behavior of a Kevlar KM2® woven fabric," *Composites Part B: Engineering*, vol. 95, pp. 144–154, 2016, doi: 10.1016/j.compositesb.2016.03.018.

[22] E. W. Lui, A. E. Medvedev, D. Edwards, M. Qian, M. Leary, and M. Brandt, "Microstructure modification of additive manufactured Ti-6Al-4V plates for improved ballistic performance properties," *Journal of Materials Processing Technology*, vol. 301, no. November 2021, p. 117436, 2022, doi: 10.1016/j.jmatprotec.2021.117436.

[23] W. Renpu, "Perforating," *Advanced Well Completion Engineering*, pp. 295–363, 2011, doi: 10.1016/b978-0-12-385868-9.00010-5.

[24] C. Huang *et al.*, "Analytical model of penetration depth and energy dissipation considering impact position," *International Journal of Impact Engineering*, vol. 191, no. March, pp. 1–14, 2024, doi: 10.1016/j.ijimpeng.2024.104997.

[25] P. Kędzierski, A. Morka, S. Stanisławek, and Z. Surma, "Numerical modeling of the large strain problem in the case of mushrooming projectiles," *International Journal of Impact Engineering*, vol. 135, no. September 2019, 2020, doi: 10.1016/j.ijimpeng.2019.103403.

[26] T. Tjahjono, T. W. B. Riyadi, B. W. Febriantoko, Suprapto, and T. Sujitno, *Hardness optimization based on nitriding time and gas pressure in the plasma nitriding of aluminium alloys*, vol. 961 MSF. 2019. doi: 10.4028/www.scientific.net/MSF.961.112.